HIGH-SPEED CHARACTERIZATION AND MECHANICAL MODELING OF MICROSCALE, AXIAL-FLUX, PERMANENT-MAGNET GENERATORS

David P. Arnold[1], Yeun-Ho Joung[2], Iulica Zana[1], Jin-Woo Park[1], Sauparna Das[3], Jeffrey H. Lang[3], David Veazie[2], and Mark G. Allen[1]

[1]Georgia Institute of Technology, School of Electrical and Computer Engineering
[2]Clark Atlanta University, Dept. of Mechanical Engineering
[3]Massachusetts Institute of Technology, Dept. of Electrical Engineering and Computer Science

ABSTRACT

This paper reports the high-speed experimental characterization of a microscale, axial-flux, permanent-magnet (PM) generator to failure. A single-phase, open-circuit voltage of 0.9 V_{rms} was measured at 225 krpm, which corresponds to 3.3 W of DC power if the machine were connected via power electronics to a matched resistive load. Finite-element analysis was used to model and examine the mechanical design of the high-speed rotor assembly to increase the speed and, hence, output power of the device. Ultimately, rotor speeds of 325 krpm were achieved using a titanium rotor housing.

Keywords: microscale generator, power MEMS, permanent-magnet machine, finite-element analysis, failure testing

INTRODUCTION

There is a tremendous need for compact, high-performance power sources that can outperform modern batteries for use in portable electronics, standalone sensors, robotics, etc. Recently, we reported a microscale, axial-flux, permanent-magnet (PM) generator that demonstrated 2.6 W of mechanical-to-electrical power conversion and delivery of 1.1 W of DC power to a resistive load at a rotor speed of 120 krpm [1]. These initial results demonstrated that multi-watt, high-power-density, mechanical-to-electrical power conversion is achievable using miniaturized magnetic machines, but the mechanical limits of the rotating machine were not explored. Experimental testing of these limits, coupled with finite-element analysis (FEA), will not only determine the maximum output power for these machines, but will also provide insight into design optimizations to achieve higher speeds and output power.

To first order, the output power of a PM machine scales quadratically with the magnetic field, surface area, and rotational speed. Thus, in order to maintain high power density in a miniaturized PM machine, high speeds are required to compensate for their reduced size. Furthermore, assuming the machine size and magnetic field are fixed by various other design constraints (e.g. maximum size limitations, limitations of magnetic materials), maximizing the rotor speed becomes a key design goal for maximum power density.

EXPERIMENTAL

The generator, fully described in [1], is a three-phase, eight-pole, axial-flux, synchronous machine, comprising a rotor with an annular SmCo PM and FeCoV soft magnetic back iron and a stator with micromachined multi-turn Cu surface windings on a NiFeMo soft magnetic substrate, which serves as the stator back iron. As shown in Fig. 1, a high-speed spindle driven by compressed nitrogen is used to spin rotors with a controllable air gap over the surface of the stators for characterization. The spindle can support no-load rotational speeds up to ~400 krpm.

The stator, shown in Fig. 2, uses interleaved, three-phase, 2-turn/pole, ~100 μm thick, electroplated Cu windings that are dielectrically isolated from the 1-mm thick NiFeMo substrate by a 5 μm polyimide layer.

The rotor assembly contains four components: annular SmCo PM, annular FeCoV back iron, mounting adaptor, and shaft. The rotor PM and back iron are each 500 μm thick with an outer diameter (OD) of 9.5 mm and inner diameter (ID) of either 3.2 mm (large magnet) or 5.5 mm (small magnet), as shown in Fig. 3. The small magnets are concentric with the active area of the stator, whereas the large magnets have additional magnetic flux that is linked by the winding inner end turns.

Sintered SmCo magnets were purchased in the desired form factor, and the rotor back irons and mounting adaptors were conventionally milled from bulk FeCoV and poly(methyl methacrylate) (PMMA), respectively. The shafts were cut from 1.6 mm diameter Grade O-1

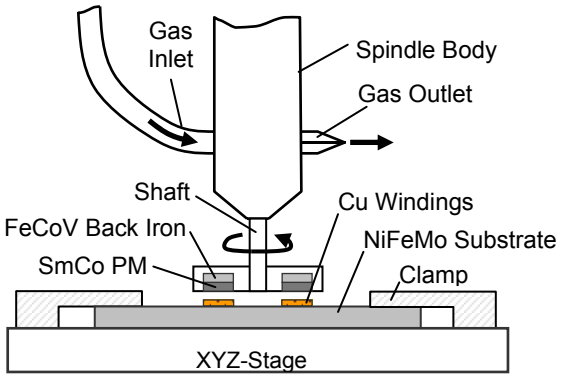

Fig. 1. Schematic of experimental test stand depicting the air-powered spindle spinning the magnetic rotor assembly over the surface of the stator.

Report Documentation Page

Form Approved
OMB No. 0704-0188

1. REPORT DATE	2. REPORT TYPE	3. DATES COVERED
2005		**00-00-2005 to 00-00-2005**

4. TITLE AND SUBTITLE	5a. CONTRACT NUMBER
High-Speed Characterization and Mechanical Modeling of Microscale, Axial-Flux, Permanent-Magnet Generators	5b. GRANT NUMBER
	5c. PROGRAM ELEMENT NUMBER
6. AUTHOR(S)	5d. PROJECT NUMBER
	5e. TASK NUMBER
	5f. WORK UNIT NUMBER
7. PERFORMING ORGANIZATION NAME(S) AND ADDRESS(ES) **Georgia Institute of Technology,School of Electrical and Computer Engineering,Atlanta,GA,30332**	8. PERFORMING ORGANIZATION REPORT NUMBER
9. SPONSORING/MONITORING AGENCY NAME(S) AND ADDRESS(ES)	10. SPONSOR/MONITOR'S ACRONYM(S)
	11. SPONSOR/MONITOR'S REPORT NUMBER(S)

12. DISTRIBUTION/AVAILABILITY STATEMENT
Approved for public release; distribution unlimited

13. SUPPLEMENTARY NOTES
The original document contains color images.

14. ABSTRACT

15. SUBJECT TERMS

16. SECURITY CLASSIFICATION OF:			17. LIMITATION OF ABSTRACT	18. NUMBER OF PAGES	19a. NAME OF RESPONSIBLE PERSON
a. REPORT	b. ABSTRACT	c. THIS PAGE			
unclassified	**unclassified**	**unclassified**		**4**	

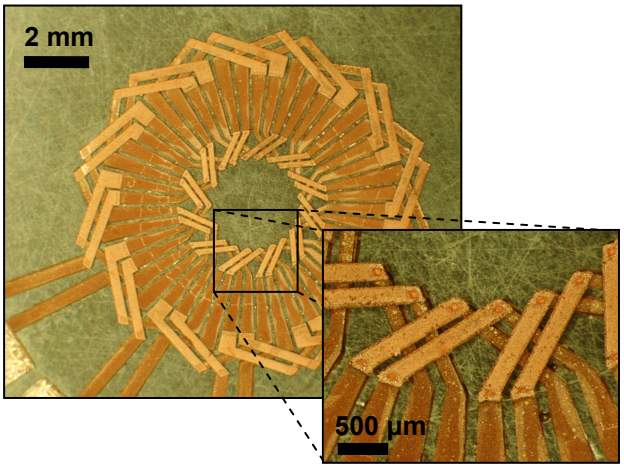

Fig. 2. Photographs of 2-turn/pole Cu stator windings.

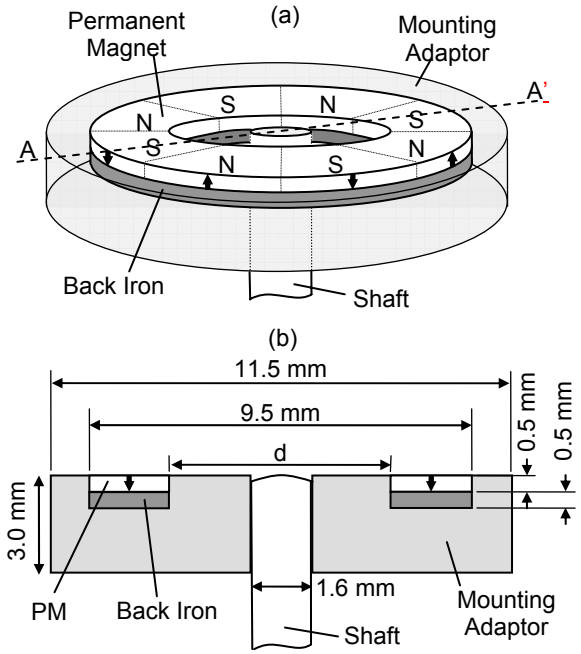

Fig. 3. Rotor assembly (a) perspective view, and (b) cross section. Magnet inner diameter, d = 3.2 mm (large magnet) or 5.5 mm (small magnet).

steel rod. After magnetizing the PM with the 8-pole magnetization pattern, the PM, back iron, and shaft were fit tightly into the mounting adaptor and glued with cyanoacrylate.

Using the small and large magnets, single-phase, open-circuit voltages were measured as a function of speed with the rotor-stator air gap (measured between top of windings and bottom of PM) set to 100 µm. As shown in Fig. 4, measurements up to 225 krpm were achieved, nearly doubling the speed of the previously reported results [1]. The voltage waveforms have sinusoidal shape and follow the expected linear trend with speed. Maximum voltages of 0.9 V_{rms} and 0.6 V_{rms} were measured for the large and small magnets, respectively, at 225 krpm.

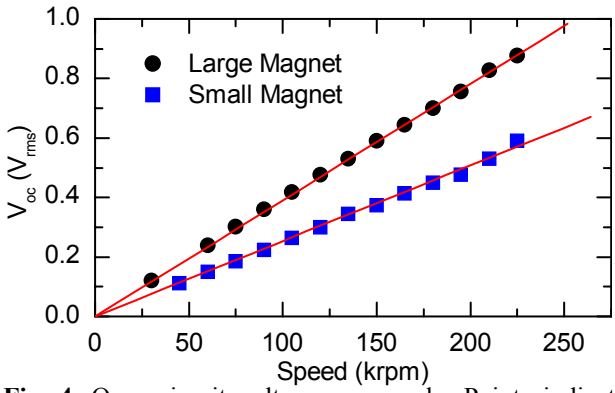

Fig. 4. Open-circuit voltage vs. speed. Points indicate measured data; lines indicate theory.

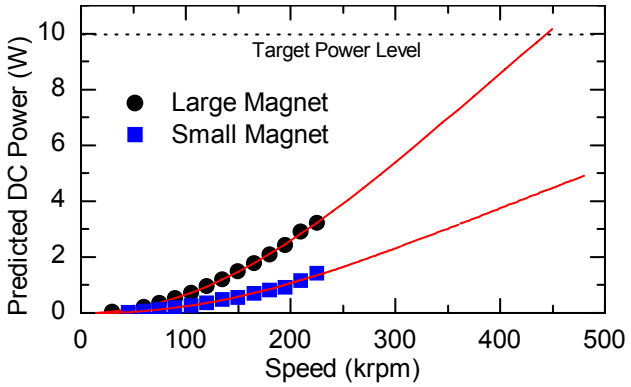

Fig. 5. Predicted DC power available to an external matched load. Points indicate values calculated from measured V_{oc} data; lines indicate theory.

Increasing the speed to ~230 krpm resulted in the mechanical fail ure of the SmCo PM and the PMMA adaptors. The PM tended to disintegrated into small pieces, and the outer retaining ring of the PMMA adaptors typically cracked and broke away. The shafts and rotor back irons remained visibly unaffected.

Using the measured open-circuit voltages as inputs to a PSpice model of the stator and power electronics [1], the theoretical output power for the three-phase generator can be predicted. Fig. 5 shows the maximum DC output power for a matched load condition. At 225 krpm, the data shows an estimated 3.3 W of DC power available for the large magnet, and 1.4 W for the small magnet. However, assuming the voltage continues to scale linearly with speed, the model indicates that 10 W could be achieved using the large magnet at a rotor speed of ~450 krpm.

Note that ideally the power should scale quadratically with speed. However, at high rotational speeds, the machine inductance, proximity effects in the transformer secondary winding resistances, and commutation effects due to the transformer secondary leakage inductance all contribute to reducing the available power [2]. These effects can be mitigated by replacing the passive power electronics with active power electronics, such as a switch mode rectifier.

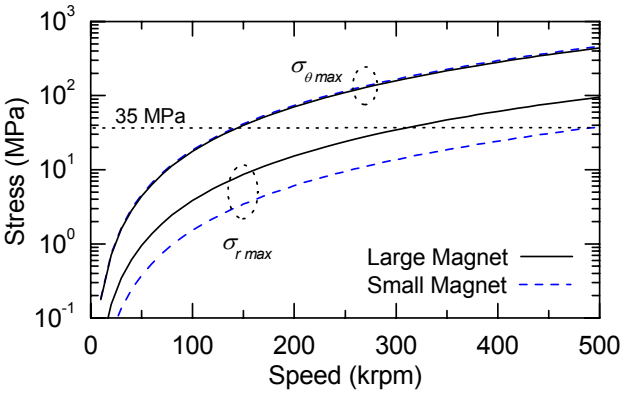

Fig. 6. Theoretical maximum hoop and radial stresses, $\sigma_{\theta\,max}$ and $\sigma_{r\,max}$, respectively, vs. speed for unconstrained large and small SmCo magnets.

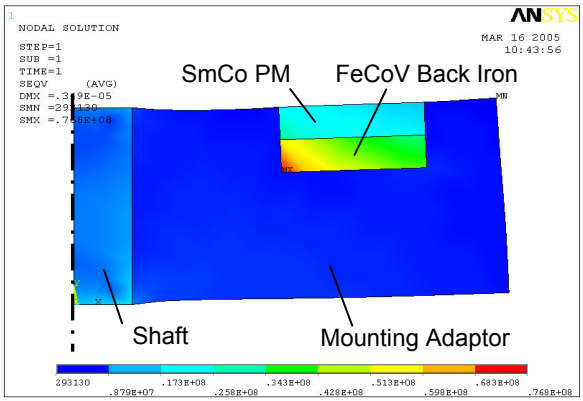

Fig. 7. FEA von Mises stress contours in the PMMA rotor assembly (Case 2) at 150 krpm.

FAILURE MODELING

Using the data from Fig. 5 as motivation for achieving higher rotational speeds, the modes of failure and the mechanical limitations of the rotor assembly were investigated. It was obvious that the low-strength, brittle SmCo was the weak point of the rotor assembly.

The maximum radial stress, $\sigma_{r\ max}$, and tangential or hoop stress, $\sigma_{\theta\,max}$, in a homogenous annulus of uniform thickness with inner radius, R_1, outer radius, R_2, spinning at angular velocity, ω, are given by [3]

$$\sigma_{r\,\max} = \sigma_r(r=\sqrt{R_1R_2}) = \frac{3+\nu}{8}\rho\omega^2\left[R_2 - R_1\right]^2, \quad (1)$$

$$\sigma_{\theta\,\max} = \sigma_\theta(r=R_1) = \frac{1}{4}\rho\omega^2\left[(3+\nu)R_2^2 + (1-\nu)R_1^2\right], \quad (2)$$

where ρ is the density and ν is the Poisson ratio for the material. Note the dependence of the stresses on the radii—$\sigma_{r\ max}$ is proportional to the square of the difference, while $\sigma_{\theta\ max}$ is related to the sum of the squares. Thus, hoop stress dominates the stresses in the system. Fig. 6 plots the stresses for unconstrained SmCo annuli for the two different rotor dimensions. The hoop stress is similar for both cases (because the outer radius dominates) and is seen to exceed the 35 MPa [4] ultimate strength for SmCo at ~140 krpm.

In the rotor assembly, the mounting adaptor provides additional stiffness to mitigate these stresses and permit higher rotational speeds. Thus, FEA was used to model the rotor assembly in order to understand the mechanics and explore the effectiveness of various rotor configurations. Titanium, with its much higher strength to density ratio, was proposed to replace the PMMA in the adaptor. More specifically, Grade 5 (Ti-6Al-4V) was chosen for its high modulus, high yield strength, and resistance to fatigue and crack propagation. Thus, four different configurations were modeled: (1) PMMA, large magnet; (2) PMMA, small magnet; (3) Ti large magnet, (4) Ti, small magnet. Simulations were performed with a 2D axisymmetric elastic-plastic model using ANSYS v9.0.

Modeling of these structures to predict failure is difficult since (1) many of the properties of these magnetic materials are not well-known; (2) irreproducible small flaws or cracks during the machining process may serve as fracture initiation points; and (3) small cracks in the magnet within a constrained outer ring structure may actually provide strain relief. Thus, these modeling results should be considered as relative guidelines for optimization rather than absolute predictors of failure.

The material properties are summarized in Table 1. The PMMA and SmCo were treated as elastic-perfectly plastic (no additional stress above the yield strength of the material), while the Ti, FeCoV, and steel were treated as purely elastic (because all stresses were below the yield strength of the materials). The simulations were performed under the following assumptions: (1) perfectly bonded mechanical interfaces; (2) perfect axisymmetric geometry from the center axis of spindle; and (3) no radial or axial displacement at the center of the spindle shaft.

The FEA indicated that inclusion of the mounting adaptor did, in fact, reduce the stresses in the SmCo. Fig. 7 shows the von Mises stress contours for the PMMA adaptor with small magnet (Case 2) at 150 krpm. The stresses in the SmCo are well below the 35 MPa limit. The FEA also confirmed that hoop stress in the SmCo was the primary cause for failure. Fig. 8 shows the stress contours in the SmCo (Case 2) as the speed is increased to 175, 200, and 225 krpm. This sequence shows the stresses building from the inner radius of the magnet, and

Table 1. Material properties used for FEA.

	Density (kg/m^3)	Modulus elasticity (GPa)	Yield strength (MPa)	Poisson's ratio
Sm_2Co_{17}	8400	117	35	0.27
PMMA	1190	3.2	50	0.35
Ti-6Al-4V (Grade 5)	4430	114	790	0.36
$Fe_{49}Co_{49}V_2$ (Hiperco 50)	8120	207	1275	0.33
Steel (Grade O-1)	7800	210	1240	0.29

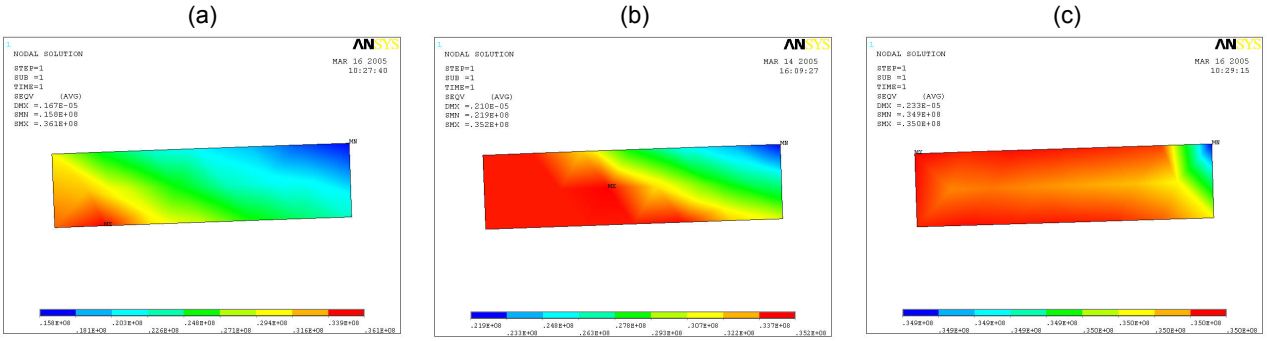

Fig. 8. FEA von Mises stress contours in the SmCo PM (Case 2) at (a) 175, (b) 200, and (c) 225 krpm.

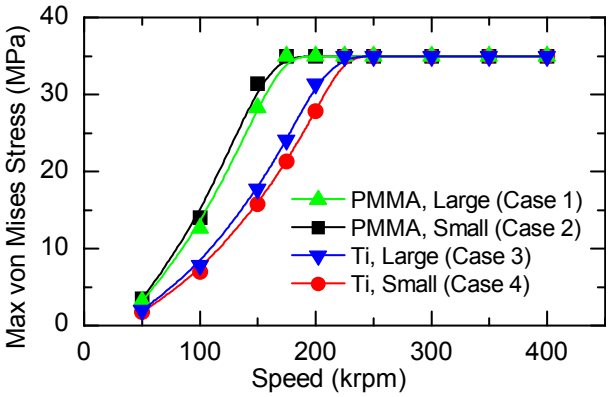

Fig. 9. Maximum FEA von Mises stress in the SmCo PM vs. speed for the four different rotor configurations.

at 225 krpm, the entire magnet has reached the 35 MPa ultimate strength. In spite of the many assumptions in the FEA, these results correlate fairly well with the measured failure speed of 230 krpm.

Fig. 9 shows the maximum von Mises stress in the SmCo PM as a function of speed for the four simulated rotor configurations. The shape of these curves provides some insight into the effectiveness of the various rotor configurations. The use of Ti clearly indicates a reduction in stress and thus should allow higher speeds. Also, there seems to be little difference in the stresses between the large and small magnets. Therefore, from a power standpoint, it would be preferred to use the large magnet.

Spinning tests were performed using a Ti adaptor and small magnet (Case 4) for comparison with the FEA. While no electrical measurements were made, the rotor achieved a maximum speed of 325 krpm without failure. The speed could not be increased because of pressure limitations from the air-driven spindle.

Table 2 summarizes two speed metrics from the FEA and the corresponding experimental failure speed for the four different rotor configurations. FEA speed 1 is the speed when any part of the SmCo PM first reaches 35 MPa (see Fig. 9). FEA speed 2 is the speed when the entire SmCo PM has reached 35 MPa.

CONCLUSIONS

A microscale, axial-flux, permanent-magnet generator was tested to failure to determine the maximum operating speeds. A maximum open-circuit output voltage of 0.9 V_{rms} was achieved at 225 krpm, corresponding to an estimated DC output power of 3.3 W. At 230 krpm, hoop stress in the SmCo PM exceeded the ultimate strength of the material, thus leading to catastrophic failure. In order to further increase the speed, the PMMA rotor housing was replaced with titanium, and maximum speeds of 325 krpm were demonstrated. Higher speeds and higher output power may be possible by further reinforcement of the rotor assembly and/or by segmenting the SmCo PM into pieces to reduce the hoop stress. Additional power increases are also possible by optimization of the machine geometry and/or power electronics.

Table 2. Rotor assembly configurations and speeds.

Case	Adaptor	Magnet	FEA speed 1* (krpm)	FEA speed 2* (krpm)	Exper. failure speed (krpm)
1	PMMA	Large	175	250	230
2	PMMA	Small	175	225	230
3	Ti	Large	225	300	--
4	Ti	Small	225	300	>325

* Note: rounded to nearest 25 krpm

ACKNOWLEDGEMENTS

This work was supported by the United States Army Research Laboratory Collaborative Technology Alliance (DAAD19-01-2-0010). The authors thank Florian Herrault, Preston Galle, and the Microelectronics Research Center staff at Georgia Tech for their assistance with fabrication.

REFERENCES

[1] S. Das, et al., "Multi-watt electric power from a microfabricated permanent-magnet generator," *Tech. Dig. 18th IEEE Int. Conf. Micro Electro Mechanical Systems* (*MEMS 2005*), pp. 287-90, Miami Beach, FL, USA, Jan. 2005.

[2] J. G. Kassakian, M. F. Schlecht, and G. C. Verghese, Principles of Power Electronics; Addison Wesley, Reading, MA, USA, 1991.

[3] W. C. Young, Roark's Formulas for Stress & Strain, 6th Ed.; p. 704, McGraw-Hill, New York, 1989.

[4] "MMPA Standard No. 0100-00, Standard Specifications for Permanent Magnet Materials," International Magnetics Association.